

Article

Nicotine Affects Multiple Biological Processes in EpiDerm™ Organotypic Tissues and Keratinocyte Monolayers

Giovanna L. Pozuelos¹, Matine Rubin¹, Samantha Vargas¹, Erik Ramirez¹, Dhiresh Bandaru¹, Jihui Sha², James Wohlschlegel² and Prue Talbot^{1,*} 

¹ Department of Molecular, Cell and Systems Biology, University of California, Riverside, CA 92521, USA; gpozu001@ucr.edu (G.L.P.); mrubi017@ucr.edu (M.R.); svarg050@ucr.edu (S.V.); erami172@ucr.edu (E.R.); sband011@ucr.edu (D.B.)

² Department of Biological Chemistry, David Geffen School of Medicine at University of California, Los Angeles, CA 90095, USA; jsha@mednet.ucla.edu (J.S.); jwohl@ucla.edu (J.W.)

* Correspondence: talbot@ucr.edu; Tel.: +1-951-827-4206

Abstract: Dermal exposure to nicotine is common due to the widespread use of tobacco products. Here, we assessed the effects of nicotine at concentrations found in thirdhand smoke (THS) contaminated environments and electronic cigarette (EC) spills or leaks on a 3D human skin model (EpiDerm™) and on submerged keratinocyte cultures. Air liquid interface treatment of EpiDerm™ with 10 or 400 µg/mL of nicotine for 24 h followed by proteomics analysis showed altered pathways related to inflammation, protein synthesis, cell–cell adhesion, apoptosis, and mitochondrial function. Submerged cultured keratinocytes were used to validate the proteomics data and further characterize the response of skin cells to nicotine. Mitochondrial phenotype changed from networked to punctate in keratinocytes treated with 10 or 400 µg/mL of nicotine for 48 h and 24 h, respectively. After 72 h, all concentrations of nicotine caused a significant decrease in the networked phenotype. In Western blots, keratinocytes exposed to 400 µg/mL of nicotine had a significant decrease in mitofusin 2, while mitofusin 1 decreased after 72 h. The shift from networked to punctate mitochondria correlated with a decrease in mitofusin 1/2, a protein needed to establish and maintain the networked phenotype. Mitochondrial changes were reversible after a 24 h recovery period. Peroxisomes exposed to 400 µg/mL of nicotine for 24 h became enlarged and were fewer in number. Nicotine concentrations in THS and EC spills altered the proteome profile in EpiDerm™ and damaged organelles including mitochondria and peroxisomes, which are involved in ROS homeostasis. These changes may exacerbate skin infections, inhibit wound healing, and cause oxidative damage to cells in the skin.

Keywords: nicotine; thirdhand smoke; electronic cigarettes; skin; EpiDerm™; dermal exposure; keratinocytes; mitochondria; peroxisomes



Citation: Pozuelos, G.L.; Rubin, M.; Vargas, S.; Ramirez, E.; Bandaru, D.; Sha, J.; Wohlschlegel, J.; Talbot, P. Nicotine Affects Multiple Biological Processes in EpiDerm™ Organotypic Tissues and Keratinocyte Monolayers. *Atmosphere* **2022**, *13*, 810. <https://doi.org/10.3390/atmos13050810>

Academic Editors: Bo Hang and Jian-Hua Mao

Received: 11 April 2022

Accepted: 12 May 2022

Published: 16 May 2022

Publisher's Note: MDPI stays neutral with regard to jurisdictional claims in published maps and institutional affiliations.



Copyright: © 2022 by the authors. Licensee MDPI, Basel, Switzerland. This article is an open access article distributed under the terms and conditions of the Creative Commons Attribution (CC BY) license (<https://creativecommons.org/licenses/by/4.0/>).

1. Introduction

The consumption of tobacco products, such as combustible cigarettes and electronic cigarettes (ECs), contributes to environmental contamination by nicotine, a highly addictive chemical that can cause adverse responses in humans [1,2]. When internalized, nicotine can be fatal in both adults and children at concentrations of 30–60 mg and 10 mg, respectively [3–5]. Uptake of environmental nicotine can occur through inhalation, ingestion, or/and dermal contact. Dermal absorption of nicotine has been of interest due to occupational exposure during the harvesting of tobacco leaves [6] and the introduction of nicotine patches [7]. In both these examples, nicotine is readily absorbed through the skin, and in the case of the tobacco harvesters, causes nausea, dizziness, and increases in heart rate and blood pressure [6,7]. In spite of prior work on green tobacco disease and nicotine patches, very little is known about how the skin responds to nicotine at concentrations found in thirdhand smoke (THS) and EC fluids.

THS is the tobacco smoke residue that settles on indoor surfaces or clothing after smoking has stopped. THS may accumulate over long periods of time [2,8–10] and may react with chemicals, such as HONO, to form carcinogens [11]. Nicotine, which is a dominant chemical in THS [12–14], has been detected on surfaces in smokers' homes and in homes of previous smokers [10]. Nicotine in THS can contact skin when contaminated clothing or surfaces are touched, leading to dermal exposure and uptake [15]. Cotinine, a nicotine metabolite, was detected in the urine of children who live in THS-contaminated households [16]. We have previously shown that in humid conditions nicotine is more readily extractable from fabrics, suggesting that exposure to nicotine could be greater in humid environments [14].

ECs are nicotine delivery devices which have gained popularity during the last 10 years. EC liquids (e-liquids) often contain high concentrations of nicotine; for example, JUUL™ fluids have ~60 mg/mL [17–19], although many earlier-generation products typically had 1–25 mg/mL [18]. EC users often come into contact with nicotine when handling products, when fluids spill, or when touching surfaces contaminated with EC fluids or residue [20–23]. In vitro studies have demonstrated transmembrane absorbance of nicotine from e-liquids [24], although its effects have not been characterized. Nicotine exposure from e-liquid spills have been reported in vape shops [20], and significant amounts of nicotine (4.571 g of nicotine/168.75 cm² fabric) accumulated in a vape shop during a month of monitoring [23]. In addition, many EC products are leaky, and users come into contact with nicotine when handling ECs [22,23].

The purpose of this study was to examine the effect of nicotine on human skin using two in vitro models. First, we exposed EpiDerm™ tissue, a three-dimensional organotypic model of human epidermis, to nicotine at concentrations found in environmental settings (THS-contaminated areas, vape shops, and EC fluids) and examined the effect of exposure on the EpiDerm™ proteome. Exposures were performed at the air liquid interface (ALI) to replicate exposures humans would receive in field sites or when using ECs. We then used cultured monolayers of human keratinocytes to validate the proteomics data and to study the cellular responses to nicotine in more detail.

2. Materials and Methods

2.1. EpiDerm™ Treatment with Nicotine

EpiDerm™ (EPI-200), produced by Mat-Tek Corporation (Ashland, MA, USA), was used to analyze the effect of nicotine on a 3D human skin model. EpiDerm™ is a ready-to-use, highly differentiated 3D tissue model consisting of normal, human-derived epidermal keratinocytes grown on tissue culture inserts. EpiDerm™ allows topical application of chemicals at the ALI and is widely used for highly predictive in vitro applications [25,26]. EpiDerm™ was shipped on cell-culture inserts in agarose. Upon receiving, inserts were removed from the agarose and incubated overnight in 0.9 mL EPI-100-NMM medium at 37 °C, 5% CO₂. The following day, the culture medium was exchanged, and the apical surface of the tissues treated with PBS (phosphate-buffered saline) only, 100 µg/mL (Nic100) or 400 µg/mL (Nic400) liquid nicotine (catalog N3876, Sigma-Aldrich, St. Louis, MO, USA) diluted in PBS. A mesh was positioned on top of the tissue to assure equal distribution of the nicotine. Inserts were treated for 24 h, after which EpiDerm™ tissues were lysed in 0.25% sodium deoxycholate, 1.0% nonidet P-40 in Mol Bio H₂O, 100 mM triethylammonium bicarbonate (TEAB) with 2 mM phenylmethylsulfonyl fluoride (PMSF) and 25 µL of Halt Cocktail.

2.2. Sample Preparation for Proteomics

2.2.1. Sample Digestion

Samples were analyzed at the UCLA proteomics core. Briefly, EpiDerm™ protein samples were mixed with an equal volume of digestion buffer (8M urea, 0.1M Tris-HCl pH 8.5). Each sample was reduced and alkylated via sequential 20 min incubations with 5 mM tris(2-carboxyethyl)phosphine (TCEP) and 10 mM iodoacetamide at room temperature in the

dark while being mixed at 1200 rpm in an Eppendorf thermomixer. Carboxylate-modified magnetic beads (CMMB), also known as SP3 [27] and ethanol (50% final concentration), were added to each sample to induce protein binding to CMMB beads. CMMB beads were washed 3 times with 80% ethanol and then resuspended with 100 mM TEAB. Protein samples were digested overnight with 0.1 µg LysC (Promega, Madison, WI, USA) and 0.8 µg trypsin (Pierce, Thermo Fisher Scientific, Waltham, MA, USA) at 37 °C.

2.2.2. TMT Labeling and CIF Fractionation

Next, 100% acetonitrile was added to each sample to make the final concentration 35%. Then, we resuspended the Tandem Mass Tag (TMT) labels with 100% acetonitrile. Next, 50 µg of each sample was labeled using TMT10plex (Thermo Fisher Scientific, Waltham, MA, USA) and the resulting nine labeled samples were pooled. The pooled sample was fractionated by CMMB-based Isopropanol Gradient Peptide Fractionation (CIF) method [28] into 6 fractions before MS analysis.

2.2.3. LC-MS Acquisition and Analysis

Fractionated samples were separated on a 75 µM ID × 25 cm C18 column packed with 1.9 µM C18 particles (Dr. Maisch GmbH) using a 140 min gradient of increasing acetonitrile and eluted directly into a Thermo Orbitrap Fusion Lumos mass spectrometer where MS spectra were acquired using SPS-MS3.

Protein identification was performed using MaxQuant [29] v 1.6.17.0. The complete human reference proteome from EMBL (UP000005640_9606 HUMAN Homo sapiens, 20,874 entries) was searched for matching MS/MS spectra. Searches were performed using a 20 ppm precursor ion tolerance. TMT10plex was set as a static modification on lysine and peptide N terminal. Carbamidomethylation of cysteine was set as static modification, while oxidation of methionine residues and N-terminal protein acetylation were set as variable modifications. LysC and trypsin were selected as the enzyme specificity with a maximum of two missed cleavages allowed. A 1% false discovery rate was used as a filter at both protein and peptide-spectrum match (PSM) levels.

Statistical analysis was conducted with the MSstatsTMT Bioconductor package [30]. The abundance of proteins missing from one condition but found in more than two biological replicates of the other condition for any given comparison were estimated by imputing intensity values from the lowest observed reporter ion intensity across samples and *p*-values were randomly assigned to those between 0.05 and 0.01 for illustration purposes.

2.3. Keratinocyte Culturing

A keratinocyte cell line transformed with human papillomavirus 16 (ATCC[®] CRL-2309TM, Manassas, VA, USA) was cultured in poly-L-lysine coated flasks using keratinocytes-serum free medium (GIBCO 17005-042, Thermo Fisher Scientific, Waltham, MA, USA) with added keratinocyte supplements (Gibco 37000-015) and Bovine Pituitary Extract (BPE; Gibco 13028-014). Cells were cultured in a 37 °C/5% CO₂/95% relative humidity incubator for 24 to 48 h before processing the cells for experiments. In experiments, keratinocytes were dispersed into single cells and seeded at a density of 100,000 cells/well in an Ibidi µ-Slide 8 Well (#80826, Ibidi GmbH, Gräfelfing, Germany). Cells were counted using a hemocytometer.

2.4. Cell Transfection

Keratinocytes were transiently transfected with sfGFP-Peroxisomes-2 (Plasmid #54601) and pMitoTimer (Plasmid #52659) purchased from Addgene (Cambridge, MA USA). Cells were transfected using a NEPA21 electron-kinetic transfection system (Bulldog Bio). Briefly, 10⁶ cells were electroporated with 10 µg/mL of sfGFP-Peroxisomes-2 and pMitoTimer plasmids. After transfection, cells were distributed equally (100,000 cells/well) into Ibidi chamber slides in keratinocytes-serum free medium (GIBCO 17005-042) with added keratinocyte

supplements (Gibco 37000-015) and Bovine Pituitary Extract (BPE; Gibco 13028-014). Cells reached 70–80% confluency prior to nicotine treatment.

2.5. Mitochondrial Morphology Analysis

Keratinocytes, transfected with the pMitoTimer plasmid were treated with nicotine concentrations found in THS-contaminated environments and in EC liquid spills or leaks (10 µg/mL (Nic10), 100 µg/mL (Nic100), 400 µg/mL (Nic400)) [15,23] for 24, 48, and 72 h prior to live cell imaging. Each cell was classified manually into three different clusters based on mitochondrial morphology. Cells with mitochondrial networks and at least 60 punctate mitochondria were categorized as “network”; cells with mitochondrial networks and more than 60 punctate mitochondria were classified as “network and punctate”; cells with only punctate and swollen mitochondria were classified as “punctate and swollen”.

2.6. Peroxisome Morphology Analysis

After transfection with sfGFP-Peroxisomes-2 plasmid, keratinocytes were treated with Nic10, Nic100, Nic400 of nicotine for 24 h. Peroxisome image analysis was performed manually using ImageJ [30]. Each peroxisome was traced using ImageJ to acquire peroxisome total area and the number of peroxisomes/cell [31].

2.7. Fluorescence Microscopy

Live cell imaging was performed using an Eclipse Ti microscope (Nikon Instruments, Melville, NY, USA) with a 60× objective. Images were captured with a high-resolution Andor Zyla VSC-04941 camera (Andor Technology, Belfast, UK). For live cell imaging, cells were maintained in a humidity-regulated incubation chamber (Pathology Devices Inc., San Diego, CA, USA) at 37 °C, 5% CO₂, and 90% relative humidity. Only cells transfected with sfGFP-Peroxisomes-2 were stained with a nuclei live cell probe, NucBlue™ Live ReadyProbes™ (Thermo Fisher Scientific, Waltham, MA, USA) 10 min prior to live cell imaging.

2.8. Western Blot

Keratinocytes were plated at a concentration of 100,000 cells/well in 6-well plates. Cells were attached for 24 h prior to treatment with Nic10, Nic100, and Nic400. After treatment, plates were placed on ice, washed with PBS to remove medium residue, and 100 µL of Radio-Immunoprecipitation Assay (RIPA) buffer with protease inhibitor cocktails (ChemCruz, Dallas, TX, USA) was added to each well. The cells were scraped using a plastic cell scraper, collected, and incubated at 30 min at 4 °C on a plate shaker. The cells were spun at 16,000× g for 15 min in a 4 °C precooled centrifuge, and the supernatant was transferred to a fresh tube kept on ice. Protein concentration was performed using the Pierce BCA assay (Thermo Fisher Scientific, Waltham, MA, USA). Laemmli buffer (Bio-Rad, Hercules, CA, USA) was added to 10 µg of each sample and boiled at 95 °C for 5 min. Samples were loaded on a Mini-PROTEAN TGX Precast SDS-PAGE gel (Bio-Rad, Hercules, CA, USA) with molecular weight markers. The gel was run at 100 volts on the Bio-Rad Powerpac Basic power supply (Bio-Rad, Hercules, CA, USA). Proteins were transferred to a PVDF membrane (Bio-Rad, Hercules, CA, USA) overnight at 150 mAmps. The following day, the membrane was blocked in 5% milk in Tween in tris-buffered saline (TBST) for 30 min at room temperature. Membranes were washed 3× prior to adding the primary antibodies. Primary antibodies (Cell Signaling, Danvers, MA, USA) of mitofusin 1 (D6E2S), mitofusin 2 (D2D10) and glyceraldehyde-3-phosphate dehydrogenase (GAPDH) (14C10) (Cell Signaling, Danvers, MA, USA) were diluted in 3% albumin in TBST separately. GAPDH was used as a loading control. Each individual antibody was added to its corresponding membrane and incubated at 4 °C overnight. The membranes were washed and incubated with HRP-conjugated antirabbit secondary antibodies diluted in 5% milk in

TBST (Tris-buffered saline, 0.1% Tween 20) for 2 h at room temperature. The protein bands were imaged using Clarity Western ECL substrate (Bio-Rad, Hercules, CA, USA).

3. Results

3.1. Proteomics Analysis of EpiDermTM Treated with Nic10 or Nic400

Volcano plots show the differentially expressed proteins for the two comparisons (Nic10 vs. PBS and Nic400 vs. PBS) (Figure 1a,b). In the Nic10 vs. PBS set, a total of 352 proteins were significantly affected (206 upregulated and 146 downregulated) (Figure 1a). In the Nic400 vs. PBS set, a total of 313 proteins were significantly affected (150 upregulated and 163 downregulated) (Figure 1b). There were 110 proteins that overlapped in the Nic10 vs. PBS and Nic400 vs. PBS sets (Figure 1c). Figure 1d shows the number of proteins that were up- and downregulated in the Nic10 and Nic400 groups. When separated into up- and downregulated proteins, there were 50 overlapping proteins for downregulated and 56 for upregulated (Figure 1d).

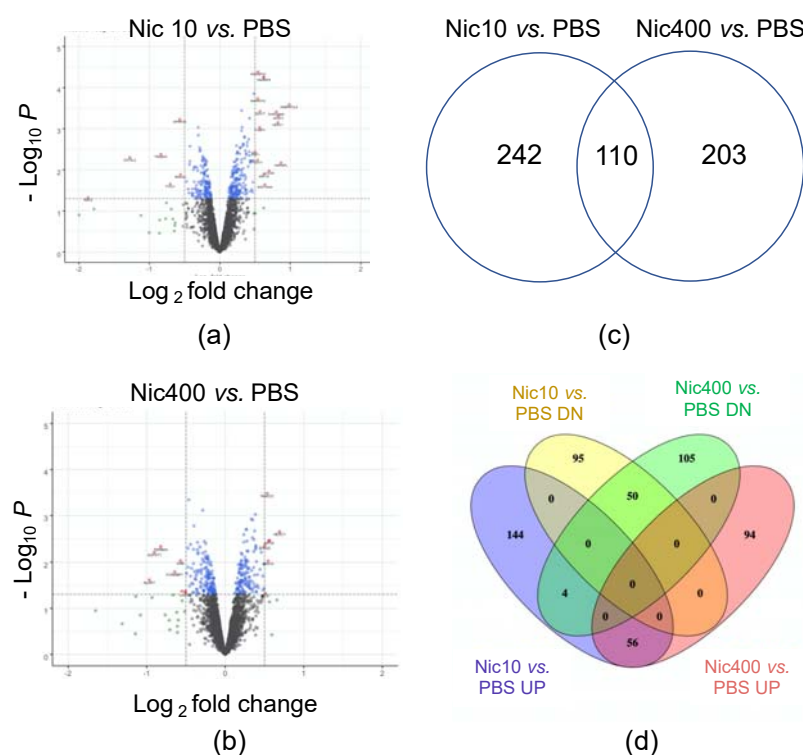


Figure 1. Volcano plots and Venn diagrams for the proteomics analysis. (a) Volcan plot for the 10 (Nic10) $\mu\text{g}/\text{mL}$ of nicotine vs. PBS comparison; (b) volcano plot for the 400 (Nic400) $\mu\text{g}/\text{mL}$ of nicotine vs. PBS comparison; (c) Venn diagram comparing proteins in the Nic10 and Nic 400 groups; (d) Venn diagram comparing up- and downregulated proteins in the Nic10 and Nic400 groups. In volcano plots, black dots = proteins not significantly affected by treatment; blue dots = significantly affected proteins with a log_2 fold-change of >0.1 ; red dots = significant affected proteins with a log_2 fold-change of >0.5 .

3.2. Canonical Pathways Affected in Nicotine-Treated EpiDermTM

The Nic10 vs. PBS set pathways with positive activated z-scores included “Protein Synthase Related Pathways” (EIF2 Signaling) and “Mitochondrial Related Pathway” (oxidative phosphorylation) (Table 1). Pathways with negative z-scores included “Apoptosis Related Pathways” (apoptosis signaling, induction of apoptosis by HIV1, TNFR1 signaling), “Cell-Cell Adhesion Related Pathway” (ILK signaling), and “Immune Related Pathways” (role of MAPK signaling in promoting the pathogenesis of influenza, IL-6 signaling, and IL-1 signaling, LPS-stimulated MAPK signaling, IL-15 production, IL-8 signaling) (Table 2).

Table 1. IPA Canonical pathways for the 10 µg/mL of nicotine vs. PBS.

Canonical Pathways	−log(<i>p</i> -Value)	z-Score	Proteins
Protein-Synthesis-Related Pathway			
EIF2 Signaling	19.2	2.53	EIF1, EIF3C, EIF3D, EIF3L, EIF4A2, MAP2K1, PTBP1, RPL15, RPL18A, RPL19, RPL24, RPL30, RPL38, RPL5, RPL6, RPL7A, RPS11, RPS13, RPS17, RPS2, RPS21, RPS24, RPS26, RPS3, RPS4X, RPS4Y2, RPS8, RPS9, RPSA
Oxidative-Stress-Related Pathway			
Oxidative Phosphorylation	4.39	1	MT-ATP6, NDUFA4, NDUFB5, NDUFB8, NDUFS1, NDUFS6, UQCRC1, UQCRC2, UQCRCQ

Table 2. Canonical Pathways for the 10 µg/mL of Nicotine vs. PBS with Negative z-scores.

Canonical Pathways	−log(<i>p</i> -Value)	z-Score	Proteins
Apoptosis-Related Pathways			
Apoptosis Signaling	3.27	−0.378	BAX, CASP7, CASP8, LMNA, MAP2K1, NFKBIB, RELA
Induction of Apoptosis by HIV1	2.73	−1.342	BAX, CASP8, FADD, NFKBIB, RELA
TNFR1 Signaling	3.17	−2.236	CASP7, CASP8, FADD, NFKBIB, RELA
Cell–Cell Adhesion-Related Pathways			
ILK Signaling	2.22	−1.342	DSP, GSK3A, ITGB4, KRT18, MTOR, RAC2, RELA, TMSB10/TMSB4X
Immune-Related Pathways			
Role of MAPK Signaling in Promoting the Pathogenesis of Influenza	1.68	−0.447	ATP6V1C1, BAX, MAP2K1, MAP2K3, NFKBIB
IL-6 Signaling	2.1	−0.816	IL36B, MAP2K1, MAP2K3, NFKBIB, RELA, TAB1
IL-1 Signaling	1.34	−1	MAP2K3, NFKBIB, RELA, TAB1
LPS-Stimulated MAPK Signaling	1.55	−1	MAP2K1, MAP2K3, NFKBIB, RELA
IL-15 Production	1.59	−1.342	CSK, MAP2K1, MAP2K3, PTK2B, RELA
IL-8 Signaling	2.04	−1.89	BAX, EIF4EBP1, MAP2K1, MTOR, NFKBIB, PTK2B, RAC2, RELA

In the Nic400 vs. PBS set, pathways included “Protein Synthesis Related Pathway” (EIF2 signaling), which had a positive z score (Table 3). Pathways with negative z scores included “Immune Related Pathways” (IL-1 signaling, ERK/MAPK signaling, MIF-mediated glucocorticoid regulation, MIF regulation of innate immunity), and “Apoptosis Related Pathway” (death receptor signaling) (Table 4).

Table 3. Canonical pathways for the 400 µg/mL of nicotine vs. PBS with positive z-scores.

Canonical Pathways	−log(p-Value)	z-Score	Proteins
Protein-Synthesis-Related Pathway			
EIF2 Signaling	6.91	2	EIF1, EIF2B2, EIF2S2, EIF3M, EIF4A2, PTBP1, RPL18A, RPL38, RPS12, RPS15, RPS24, RPS26, RPS3, RPS4X, RRAS2

Table 4. Canonical pathways for the 400 µg/mL of nicotine vs. PBS with negative z-scores.

Canonical Pathways	−log(p-Value)	z-Score	Proteins
Immune-Related Pathways			
IL-1 Signaling	2.15	−0.447	MAP2K3, NFKBIB, PRKAR1A, RELA, TAB1
ERK/MAPK Signaling	2.29	−0.707	PAK1, PLA2G4A, PLA2G4D, PPP2R5A, PRKAR1A, PRKCI, PTK2B, RRAS2
MIF-Mediated Glucocorticoid Regulation	4.05	−1.342	MIF, NFKBIB, PLA2G4A, PLA2G4D, RELA
MIF Regulation of Innate Immunity	3.6	−1.342	MIF, NFKBIB, PLA2G4A, PLA2G4D, RELA
Apoptosis-Related Pathway			
Death Receptor Signaling	1.54	−1	ARHGDIB, CASP8, NFKBIB, RELA

3.3. IPA Toxicity Analysis

Because treatment involved nicotine, a chemical with potentially harmful effects, a toxicological analysis was also performed using IPA (Table 5). The IPA toxicity list for the Nic10 vs. PBS set included terms consistent with “Mitochondrial Dysfunction” and “Oxidative Stress.” Proteins associated with “Mitochondria Dysfunction” were part of the protein complexes in the electron transport chain (NDUFA8, NDUFA9, NDUFB8, NDUFS1, NDUFS6, UQCRC1, UQCRC2). Only two proteins (MFN1, PKM) were involved in the “Decreases Respiration of Mitochondria.” Proteins involved in “Increases Transmembrane Potential of Mitochondria” and “Mitochondrial Membrane” included BAX, CASP7, DNAJB1. Proteins involved in apoptosis were downregulated (BAX, CASP7, CASP8), suggesting an anti-apoptosis response to nicotine treatment.

Table 5. Toxicity lists for the 10 µg/mL of Nicotine vs. PBS comparison.

IPA Toxicity Lists	−log(p-Value)	Proteins
Mitochondrial Dysfunction	5.41	CASP8, CPT1A, MT-ATP6, NDUFA4, NDUFB5, NDUFB8, NDUFS1, NDUFS6, PARK7, UQCRC1, UQCRC2, UQCRQ
NRF2-Mediated Oxidative Stress Response	2.27	AKR1A1, BACH1, DNAJB1, DNAJB11, DNAJB2, DNAJC11, DNAJC5, MAP2K1, MAP2K3
Decreases Respiration of Mitochondria	1.83	MFN1, PKM
Pro-Apoptosis	1.72	BAX, CASP7, CASP8
Increases Transmembrane Potential of Mitochondria and Mitochondrial Membrane	1.52	BAX, CASP7, DNAJB1
Mechanism of Gene Regulation by Peroxisome Proliferators via PPARα	1.4	MAP2K1, NFKBIB, RELA, TAB1

The IPA toxicity list for the Nic400 vs. PBS set was similar to the lower concentration (NIC10) in that it included terms related to “Mitochondrial Dysfunction” and “Oxidative Stress” (Table 6). Additional terms that appeared with the higher nicotine concentration were related to “PXR/RXR Activation”, “Hypoxia-inducible Factor Signaling”, “Aryl Hydrocarbon Receptor Signaling”, “Cholesterol Biosynthesis”, and “LXR/RxR Activation”.

Table 6. Toxicity lists for the 400 µg/mL of nicotine vs. PBS comparison.

IPA Toxicity Lists	−log(p-Value)	Proteins
Mitochondrial Dysfunction	4.34	CASP8, COX7A2, COX7C, NDUFA4, NDUFA8, NDUFA9, NDUFB5, NDUFS1, TXN2, UQCRCQ
PXR/RXR Activation	2.95	GSTM2, PCK2, PRKAR1A, RELA, SCD
NRF2-Mediated Oxidative Stress Response	2.59	AKR1A1, BACH1, CDC34, DNAJC13, DNAJC5, GSTM2, MAP2K3, PRKCI, RRAS2
Mechanism of Gene Regulation by Peroxisome Proliferators via PPARα	2.23	FAT1, NFKBI, PRKAR1A, RELA, TAB1
Decreases Depolarization of Mitochondria and Mitochondrial Membrane	2.07	PAK1, PLA2G4A, PPIA
Hypoxia-Inducible Factor Signaling	1.99	EIF1, EIF2B2, EIF2S2, UBE2N
RAR Activation	1.91	PRKAR1A, PRKCI, PRMT1, RDH12, RELA, SDR16C5, SMARCC2
Aryl Hydrocarbon Receptor Signaling	1.87	ALDH3A1, CDKN2A, CTSD, GSTM2, NEDD8, RELA
Cholesterol Biosynthesis	1.81	IDI1, SQLE
LXR/RXR Activation	1.77	ACACA, IL36B, PLTP, RELA, SCD
Oxidative Stress	1.5	GSTM2, RELA, S100A7

3.4. Nicotine Alters Mitochondrial Morphology in Human Keratinocytes

Based on the IPA canonical pathways and toxicity lists, mitochondria were identified as targets of nicotine at both treatment concentrations. Mitochondrial morphology was further assessed in vitro using human keratinocytes transfected with the MitoTimer plasmid that specifically labels mitochondria and enables mitochondrial morphology to be evaluated (Figure 2a–l). Mitochondria in control cells were generally elongated networks (Figure 2a–c), while cells in treated groups appeared to have more punctate mitochondria, which were sometimes swollen (Figure 2d–l).

Mitochondrial phenotypes were quantified in each group (Figure 2m–o). In keratinocytes treated with Nic400 for 24, 48, or 72 h, there was a decrease in the percent of mitochondria with “network” morphology at all times and a corresponding increase in the percentage with “network and punctate” (24 h) and “punctate and swollen” (48 and 72 h) (Figure 2j–o). In the Nic10-treated group, “network” morphology decreased (48 and 72 h) and “network and punctate” morphology increased (48 h). In the Nic100-treated group, network morphology decreased following 48 and 72 h treatments. These data show that nicotine induces a progressive time- and dose-dependent transition from mainly networked mitochondria to the punctate and swollen form in human keratinocytes.

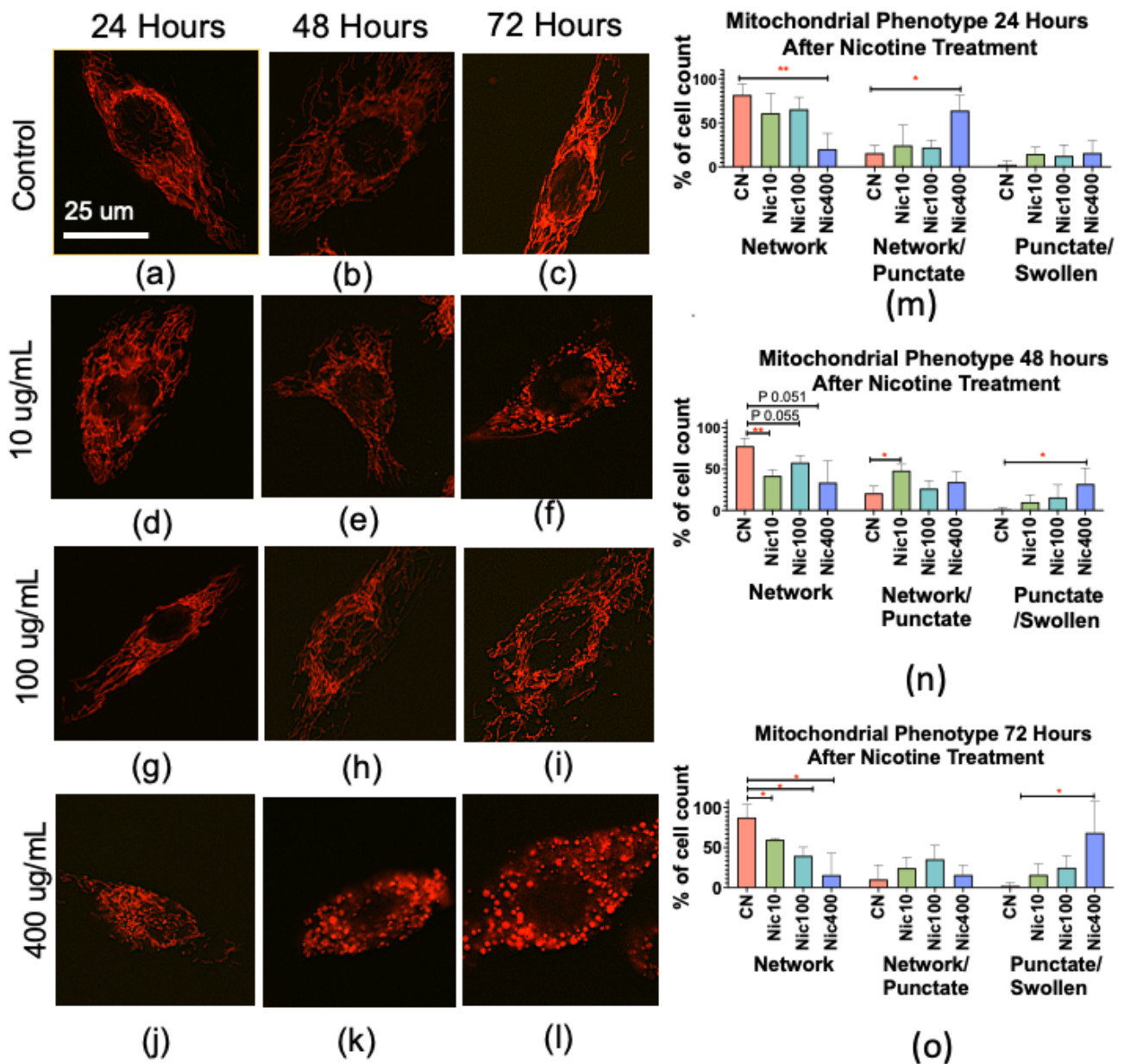


Figure 2. Mitochondria in keratinocytes treated with Nic10, Nic100, or Nic400 for 24, 48, or 72 h. (a–l) Micrographs of mitochondria treated with various concentrations of nicotine and imaged at different times; (m) mitochondrial morphology 24 h after nicotine treatment; (n) mitochondrial morphology 48 h after nicotine treatment; (o) mitochondrial morphology 72 h after nicotine treatment. CN = control medium. All data are means ± the standard error of the mean for three independent experiments. * = $p < 0.05$, ** = $p < 0.01$.

3.5. Mitofusin 1/2 Decreased in Keratinocytes Treated with Nic400

Mitochondria normally undergo cyclic fusion and fission, which are regulated by the mitofusins 1 and 2 [32]. The previous experiment suggested that nicotine impaired mitochondrial fusion, which would favor an increase in the punctate form. We tested the hypothesis that nicotine suppressed the expression of mitofusins 1/2 using Western blotting. Mitofusin 1 levels decreased after 72 h in the Nic400 group (Figure 3a–c). Mitofusin 2 levels significantly decreased in the Nic400 group at all exposure times (Figure 2d–f).

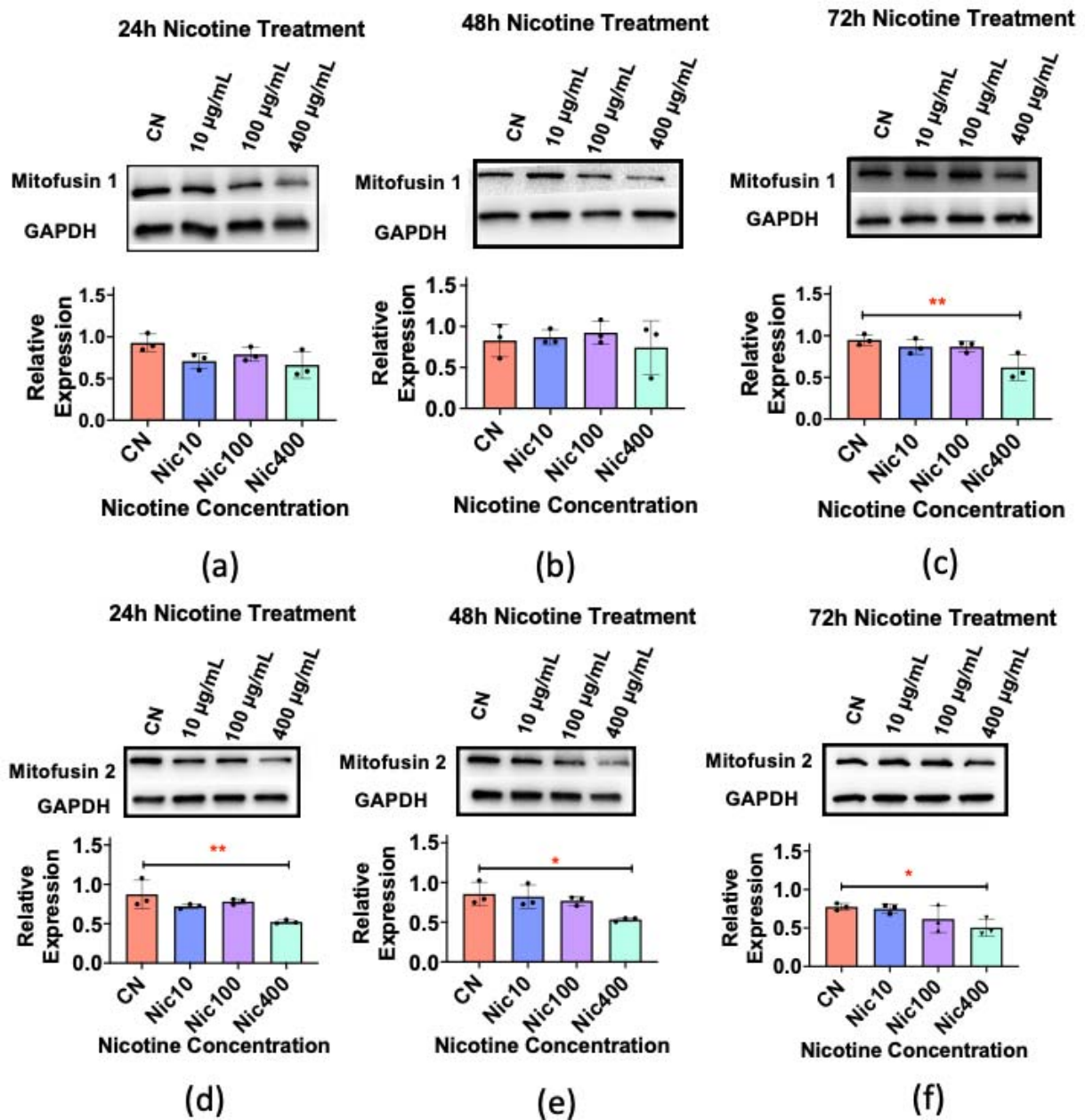


Figure 3. Mitofusin 1/2 protein in keratinocytes after nicotine treatment. Mitofusin 1 in Western blots after 24 h (a); 48 h (b); and 72 h (c) of nicotine treatment. Mitofusin 2 in Western blots after 24 h (d); 48 h (e); and 72 h (f) of nicotine treatment. CN = control medium. All data are means ± the standard error of the mean for three independent experiments represented by black dots. * = $p < 0.05$, ** = $p < 0.01$.

3.6. Recovery of Mitochondrial Morphology in Keratinocytes after Nicotine Treatment

To determine if the changes observed in mitochondrial morphology and mitofusin levels were reversible, a follow up experiment was performed, in which cells were treated with Nic400 and allowed to recover in nicotine-free medium for 24 or 48 h. The percent of “network” and “network and punctate” mitochondria in the Nic400-treated group returned to control levels following a 24 or 48 h recovery period in cell medium without nicotine (Figure 4i,j). To determine if longer treatment required longer recovery periods, cells were exposed to nicotine for 48 h prior to recovery. In this case, it took 48 h for mitochondrial morphology to return to control levels (Figure 4k,l).

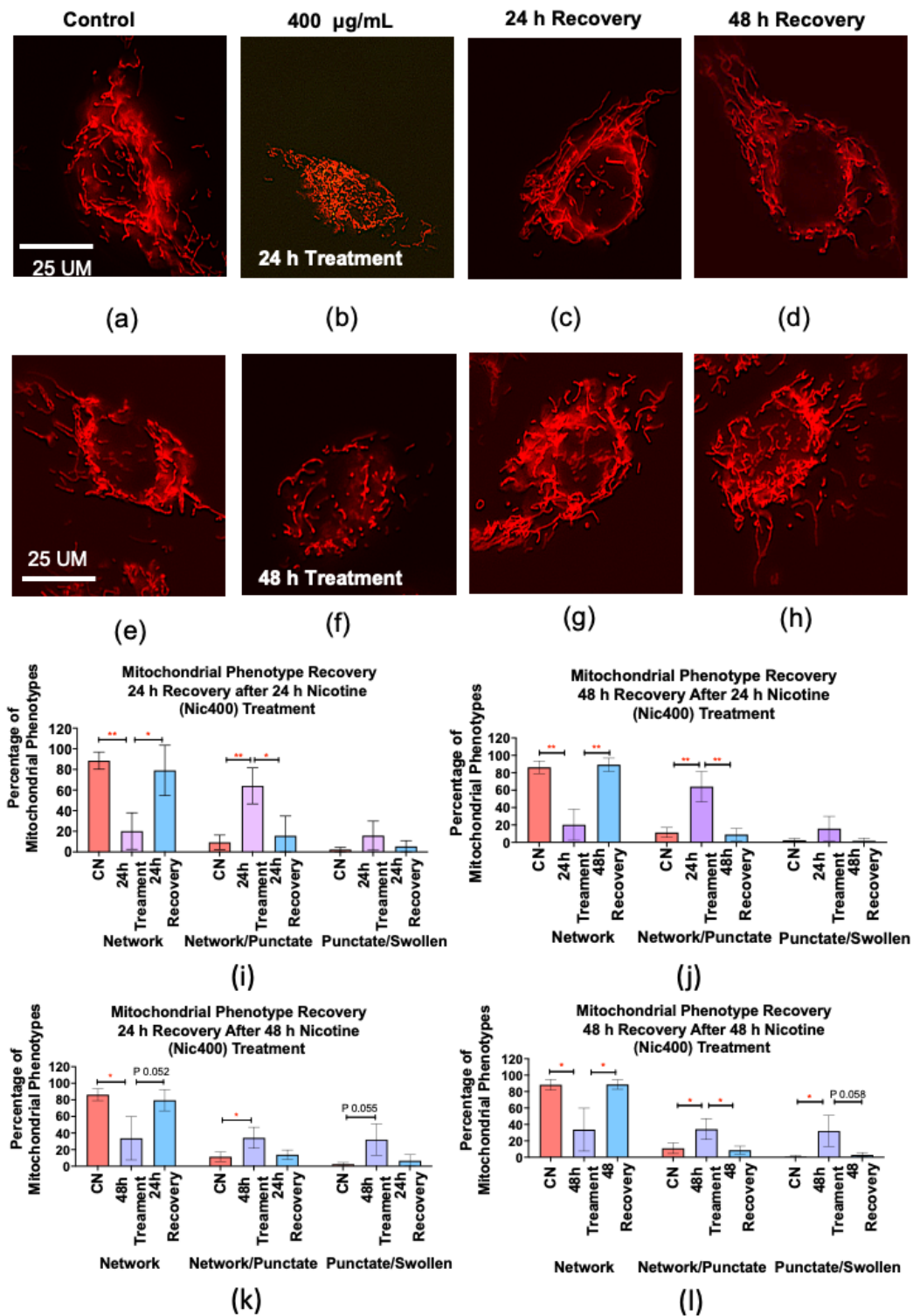


Figure 4. Mitochondrial morphology in nicotine treated keratinocytes returns to normal after 24 h and 48 h of recovery in culture medium. (a–h) Micrographs showing untreated controls, cells treated with nicotine, and cells that recovered 24 h or 48 h after treatment. (i) Mitochondrial morphology in keratinocytes treated for 24 h and after 24 h of recovery. (j) Mitochondrial morphology in keratinocytes treated for 24 h and after a 48 h recovery. (k) Mitochondrial morphology in keratinocytes treated for 48 h and after 24 h of recovery. (l) Mitochondrial morphology in keratinocytes treated for 48 hours and after 48 h of recovery. CN = Control Medium. All data are means \pm the standard error of the mean for three independent experiments. * = $p < 0.05$, ** = $p < 0.01$.

Western blots were performed to determine if mitofusin 1/2 recovered after nicotine treatment. In the Nic400-treated group, cells were exposed for 72 h to produce a decrease in mitofusin1 as shown in Figure 3c. Mitofusin 1 recovered to control levels after 24 h in culture medium without nicotine (Figure 5a). For mitofusin 2, exposure was reduced to 24 h, since this was adequate time to decrease the levels of this protein (Figure 3d). In this case, recovery to control levels occurred in 48 h (Figure 5b).

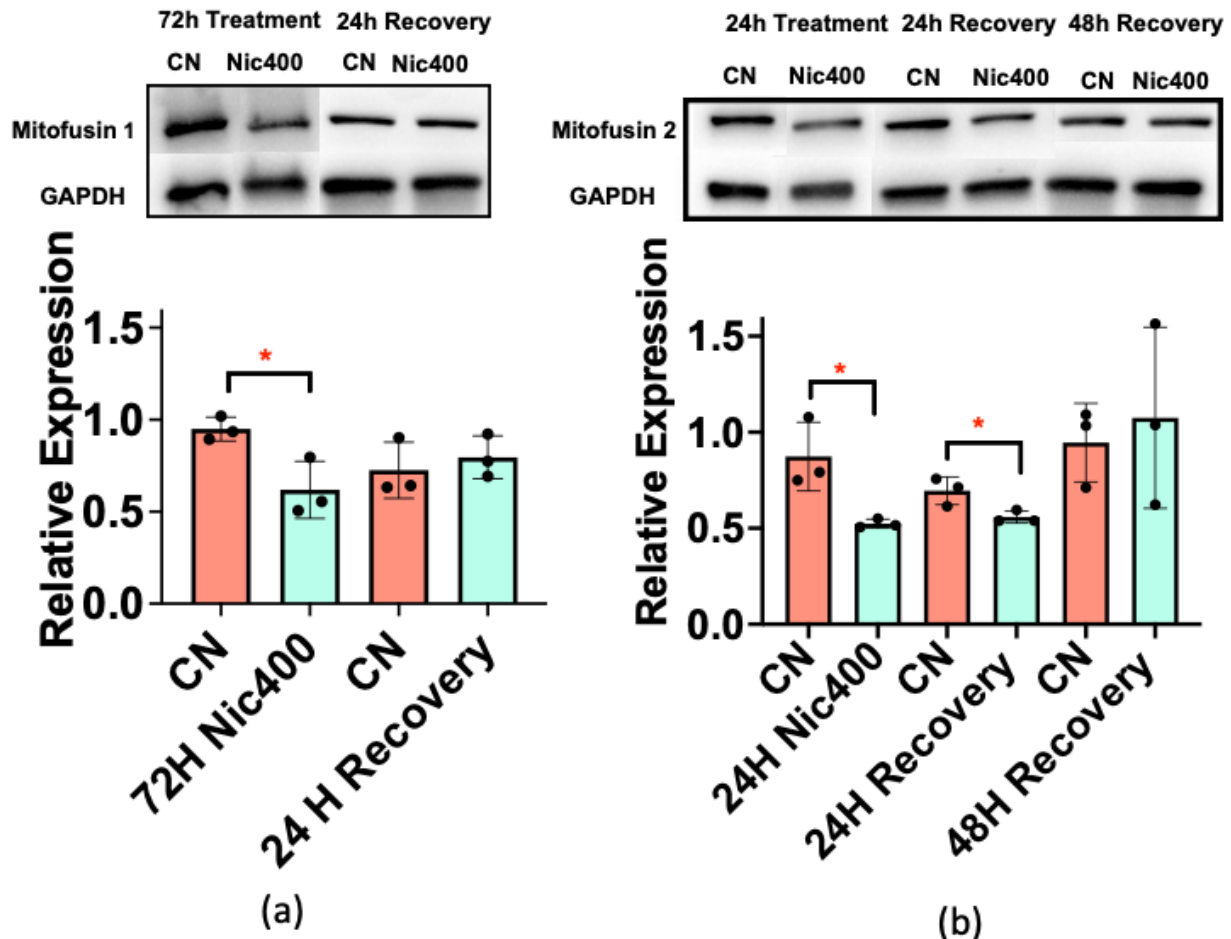


Figure 5. Mitofusin 1/2 protein expression in nicotine treated keratinocytes after 24 and 48 h of recovery. (a) Expression of mitofusin 1 in a Western blot after 72 h of exposure to Nic400 and after 24 h of recovery; (b) expression of mitofusin 2 after 24 h of exposure to Nic400, followed by 24 and 48 h of recovery. CN = control medium. All data are means \pm the standard error of the mean for three independent experiments. * = $p < 0.05$.

3.7. Nicotine Treatment Altered the Number and Size of Peroxisomes

Peroxisomes are involved in neutralizing ROS [33]. Since we observed changes in the proteomics data related to oxidative stress, we examined the effect of nicotine on peroxisomes in keratinocytes transfected with the sfGFP-Peroxisomes-2 plasmid to visualize peroxisome size and number. Peroxisome morphology was altered in keratinocytes treated with Nic400 for 24 h (Figure 6a,b). The peroxisomes in the treated cells appeared to be fewer, larger, and more fluorescent (Figure 6b). Peroxisome numbers and size were quantified manually. Nicotine treatment decreased the number of peroxisomes in all groups, with Nic400 being significantly lower than the untreated control (Figure 6c). The area of peroxisomes/cell increased in the Nic400-treated group (Figure 6d).

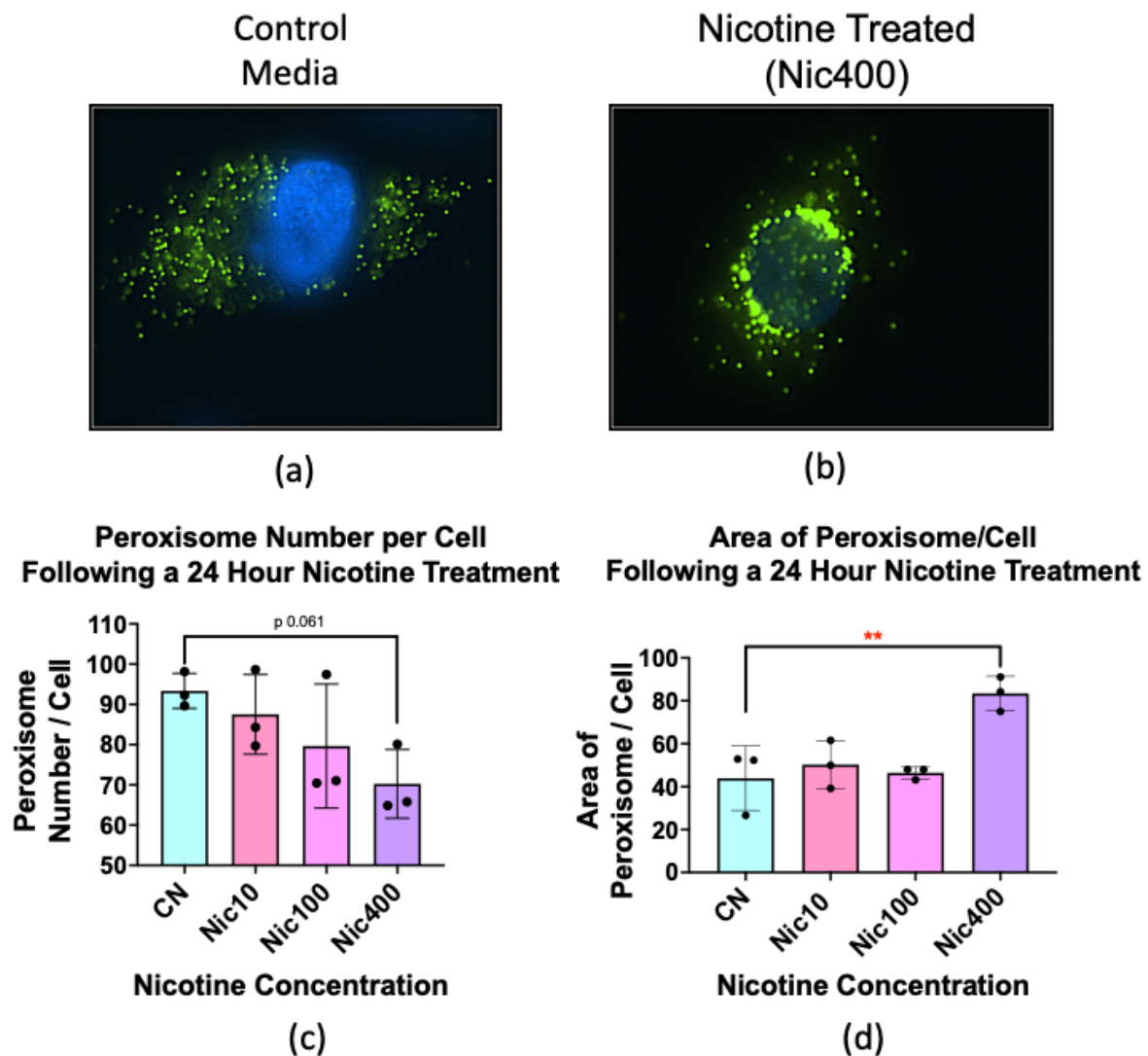


Figure 6. Peroxisome morphology in keratinocytes after nicotine treatment. (a,b) Micrographs of peroxisomes (green) in keratinocytes following treatment with (a) control medium and (b) Nic 400. (c) Number of peroxisomes per cell following treatment with control medium, Nic10, Nic100, and Nic400 for 24 h; (d) area of peroxisomes per cell following treatment with control medium, Nic10, Nic100, and Nic400 for 24 h. CN = control medium. All data are means \pm the standard error of the mean for three independent experiments. $** = p < 0.01$.

4. Discussion

The effects of nicotine in THS and EC products on human skin have not been well characterized. To our knowledge, this is the first proteomics study showing how EpiDerm™, a 3D model of human skin, responds to concentrations of nicotine found in THS and EC fluids during ALI exposure. Nicotine stimulated responses in the EpiDerm™ model that may negatively impact the skin and included: (1) an anti-inflammatory response that could promote bacterial infections and impair wound healing; (2) altered EIF2 protein synthesis that may initiate a stress response and suppress apoptosis; (3) an increase in proteins involved in oxidative phosphorylation; and (4) alterations in mitochondrial-related pathways. Cultured human keratinocytes confirmed and extended the proteomics data. The nicotine-induced responses could lead to skin damage, infections, and progression to disease.

Nicotine concentrations used in this study were comparable to those in THS-contaminated environments and EC liquid spills or leaks. The lowest concentration (Nic10) was based

on nicotine concentrations in extracts from fabrics lightly exposed to cigarette smoke over 18 months in a laboratory setting [14]. Higher concentrations (Nic100 and Nic 400) were used to simulate environmental settings without smoking bans, heavily exposed to cigarette smoke, and not frequently cleaned. The Nic400 concentration was also used to assess nicotine exposure through the handling of e-fluid, although this concentration is slightly outside the lower end of the nicotine range in e-fluids (1–60.9 mg/mL) [17–19].

At Nic10 and Nic400 concentrations, we observed inhibition of inflammatory-related pathways in the EpiDermTM skin model, similar to in vivo animal and human studies [34–38]. Although nicotine's anti-inflammatory properties may be beneficial for inflammatory skin diseases [39], such as psoriasis and atopic dermatitis, it can also facilitate bacterial infections in the skin and impair wound healing [34,36,40]. In vivo animal studies show that nicotine stimulated the cholinergic anti-inflammatory pathway and reduced antimicrobial peptide activity, allowing susceptibility to *Staphylococcus aureus* infection in the skin of mice [34,41,42]. Activation of $\alpha 7$ nAChR by nicotine inhibited the NF- κ B pathway and toll-like receptor 2 (TLR2) signaling, causing a decrease in receptor response to bacterial and other pathogens [42]. Inhibition of TLR2 activity is detrimental for proper modulation of the pro-inflammatory signals needed to initiate wound healing. Recruitment of neutrophils to wounds helps eliminate pathogens, and macrophages secrete growth factors that stimulate cell proliferation to replace damage tissue [43–45]. TLR2 signaling is also involved in stimulating cell migration for proper wound healing. In keratinocytes, migration in scratch assays was attenuated by nicotine (10^{-9} M) through activation of $\alpha 7$ nAChR and suppression of TLR2 [42]. In EpiDermTM, nicotine (Nic10) decreased cell–cell adhesion proteins consistent with an increase in cell migration. Variations in results may depend on the cell type and nicotine concentrations. We used a 3D skin model without wound incision and alteration of cell–cell adhesion proteins were only observed in Nic10 treatment. Other studies have also reported increases in cell migration in human keratinocytes at different nicotine concentrations (10^{-7} – 10^{-5} M), [46,47]. We show that EpiDermTM exposed to nicotine concentrations found in THS decreased inflammation-related pathways, which could contribute to pathogen infections and improper wound healing. In mice exposed to THS, wound healing in skin was impaired, and wounds were fragile [48]. Nicotine's anti-inflammatory properties may be the main contributor to the delay in wound healing observed in THS exposed mice [48].

Proteomics analysis of EpiDermTM treated with nicotine (Nic10 and Nic400) predicted an activated state of the EIF2 signaling pathway, which is involved in global protein synthesis. However, under stress conditions, eukaryotic translation initiation factor 2 alpha (eIF2 α) may become phosphorylated and selectively translate only a subset of mRNAs necessary for cell survival and stress recovery, such as inhibitors of apoptosis [49,50]. Nicotine phosphorylation of EIF2 is depended on treatment concentration, cell type, and experimental model [51–53]. In our 3D EpiDermTM model, increased expression of proteins involved in the EIF2 pathway may be associated with stress-related protein synthesis, since: (1) mitochondrial-stress-related pathways were also observed (Nic10); (2) apoptosis pathways were decreased; and (3) expression of RPL19, a ribosomal protein involved in the activation of the unfolded protein response, was increased [54].

Mitochondrial-related pathways were the top hit on IPA's tox list analysis in the EpiDermTM treatments. Alterations in mitochondrial dynamics and oxidative stress have been observed in cells treated with nicotine [55,56]. Nicotine binds to acetylcholine receptors in keratinocytes to stimulate a Ca²⁺ influx [57]. Proteins altered in EpiDermTM treated with nicotine included those in the electron transport chain. THS and nicotine altered mitochondrial morphology in mouse neural stem cells (mNSCs) [56]. In our study, nicotine at concentrations found in THS-exposed fabric decreased mitochondrial networks, while punctate and swollen mitochondria increased. Mitochondrial fragmentation was dependent on both nicotine concentration and time. The shift from networked to punctate mitochondria correlated with a decrease in mitofusin 1/2, proteins involved in mitochondrial fusion, which are needed to maintain the networked phenotype. A similar nicotine-induced mito-

chondrial fission accompanied by a decrease in mitofusin 1/2 was observed in neonatal rat ventricular cardiomyocytes and [55] in human multipotent embryonal carcinoma cells [58]. Mitochondrial fragmentation was reversible in human keratinocytes, suggesting skin could recuperate after THS exposure. Alterations in mitochondria could lead to ROS imbalance and oxidative stress in skin.

Changes in mitochondrial phenotype have been observed in stem cells exposed to THS, e-liquid, and nicotine [56,59]. Unlike keratinocytes, which have networked mitochondria, stem cell mitochondria are punctate and have low activity. When cells are stressed, mitochondria in mNSCs undergo fusion, a response referred to as stress-induced mitochondrial hyperfusion (SIMH), resulting in increased ATP production [59]. SIMH occurs in neural stem cells during exposure to THS, e-liquid, or nicotine, and is a survival mechanism [56,59]. Our results show that mitochondria in stem cells and differentiated keratinocytes respond differently to nicotine. Stem cells mount a survival response via SIMH, while mitochondria fragment in differentiated keratinocytes, which may occur in parallel with a survival response initiated by EIF2.

Peroxisomes are essential for various cellular functions, including maintenance of ROS homeostasis and degradation of hydrogen peroxide [33,60,61]. Abnormalities in peroxisomes can impair catalase activity and lead to inadequate detoxification of ROS, which in turn can cause oxidative stress and contribute to impaired mitochondrial function [33]. In our study, peroxisomes in keratinocytes exposed to Nic400 showed both a decrease in number and an increase in size relative to the controls. Changes in number can be caused by increased pexophagy, which occurs when peroxisomes are damaged [62] and can be triggered by excess ROS [63]. The increase in size could be due to swelling of damaged peroxisomes, which has been reported in a PEX 11 knockout cell line [64] and in liver cells from mice with dysfunctional peroxisomes [65]. Swelling may also occur when peroxisomes are proliferating [64], which may have occurred in our system to replace those lost by pexophagy.

Dysfunctional peroxisomes can activate eIF2 transcription of stress pathways and increase ROS, leading to mitochondrial dysfunction [51,66,67]. In a mouse model with dysfunctional peroxisomes, increased phosphorylation of eIF2- α led to activation of transcription factors that regulate expression of stress-related genes [51,67,68]. EIF2 signaling was affected in our proteomics analysis and may be a response to peroxisome dysregulation. Impaired peroxisomes also increase ROS and can trigger mitochondrial dysfunction [67,69–71], which was observed in both our proteomics data and phenotype analysis of mitochondria. In keratinocytes, peroxisomes were abnormal by 24 h of treatment, while mitochondrial swelling was observed after 72 h. Our data support the conclusion that treatment of human keratinocytes with nicotine leads to peroxisome dysfunction, which may in turn activate stress responses and contribute to mitochondrial dysfunction.

Our data establish a foundation upon which future studies can be performed. We tested multiple nicotine concentrations, but they may not include all concentrations in environmental settings or EC fluids, both of which are both highly variable. Our EpiDermTM data come from one individual (male). Future studies could use gender and age matched groups and include chronic exposures.

5. Conclusions

Nicotine concentrations associated with environmental THS and ECs penetrate EpiDermTM and cultured keratinocytes and: (1) produce an anti-inflammatory response which could exacerbate skin infections and impair wound healing, (2) alter the EIF2 signaling pathway, which may activate a cellular stress response and inhibit apoptosis, (3) increase oxidative stress, and (4) alter both mitochondrial and peroxisome morphologies and disrupt ROS homeostasis. Even a short exposure to low concentrations of nicotine was sufficient to alter the EpiDermTM proteome and adversely affect organelles involved in oxidative stress. These data, in conjunction with our earlier study showing alterations in the human nasal epithelium following inhalation of THS chemicals [72], provide strong evidence that

humans are adversely affected by both dermal and inhalation exposure to THS. Together, these data demonstrate a need for a better understanding of the effects of nicotine in THS and ECs on humans, broadening restrictions on indoor smoking and vaping, and developing policies for remediating contaminated environments.

Author Contributions: Conceptualization, P.T. and G.L.P.; methodology, G.L.P., J.S. and J.W.; software, J.S., J.W., G.L.P. and M.R.; validation, G.L.P.; formal analysis, G.L.P., M.R., D.B., S.V., E.R., J.S. and J.W.; investigation, P.T. and G.L.P.; resources, P.T.; data curation, G.L.P.; writing—original draft preparation, G.L.P.; writing—review and editing, G.L.P., P.T., J.S. and J.W.; visualization, G.L.P. and M.R.; supervision, P.T.; project administration, P.T.; funding acquisition, P.T. All authors have read and agreed to the published version of the manuscript.

Funding: This project was supported by funds from the Tobacco-Related Disease Research Program California (24RT-0037), and the UCR Academic Senate. The funders had no role in study design, data collection and analysis, decision to publish, or preparation of the manuscript.

Institutional Review Board Statement: Not applicable.

Informed Consent Statement: Not applicable.

Data Availability Statement: Raw data uploaded to the proteomics repository MassIVE (accession number: MSV000089438).

Conflicts of Interest: The authors declare no conflict of interest.

References

1. Mishra, A.; Chaturvedi, P.; Datta, S.; Sinukumar, S.; Joshi, P.; Garg, A. Harmful effects of nicotine. *Indian J. Med. Paediatr. Oncol.* **2015**, *36*, 24–31. [[CrossRef](#)] [[PubMed](#)]
2. Jacob, P., III; Benowitz, N.L.; Destailats, H.; Gundel, L.; Hang, B.; Martins-Green, M.; Matt, G.E.; Quintana, P.J.E.; Samet, J.M.; Schick, S.F.; et al. Thirdhand Smoke: New Evidence, Challenges, and Future Directions. *Chem. Res. Toxicol.* **2017**, *30*, 270–294. [[CrossRef](#)] [[PubMed](#)]
3. Solarino, B.; Rosenbaum, F.; Riesselmann, B.; Buschmann, C.T.; Tsokos, M. Death due to ingestion of nicotine-containing solution: Case report and review of the literature. *Forensic Sci. Int.* **2010**, *195*, e19–e22. [[CrossRef](#)] [[PubMed](#)]
4. Tjonckje, J.A.; Goncalves, R.; Castaing, N.; Molimard, M.; Tovagliaro, F.; Titier, K. Death related to nicotine replacement therapy: A case report. *Forensic Sci. Int.* **2020**, *309*, 110223. [[CrossRef](#)]
5. Mayer, B. How much nicotine kills a human? Tracing back the generally accepted lethal dose to dubious self-experiments in the nineteenth century. *Arch. Toxicol.* **2014**, *88*, 5–7. [[CrossRef](#)]
6. McKnight, R.H.; Spiller, H.A. Green tobacco sickness in children and adolescents. *Public Health Rep.* **2005**, *120*, 602–605. [[CrossRef](#)]
7. Sørensen, L.T.; Zillmer, R.; Agren, M.; Ladelund, S.; Karlsmark, T.; Gottrup, F. Effect of smoking, abstinence, and nicotine patch on epidermal healing and collagenase in skin transudate. *Wound Repair Regen.* **2009**, *17*, 347–353. [[CrossRef](#)]
8. Matt, G.E.; Quintana, P.J.; Hovell, M.F.; Chatfield, D.; Ma, D.S.; Romero, R.; Uribe, A. Residual tobacco smoke pollution in used cars for sale: Air, dust, and surfaces. *Nicotine Tob. Res.* **2008**, *10*, 1467–1475. [[CrossRef](#)]
9. Matt, G.E.; Quintana, P.J.; Destailats, H.; Gundel, L.A.; Sleiman, M.; Singer, B.C.; Jacob, P.; Benowitz, N.; Winickoff, J.P.; Rehan, V.; et al. Thirdhand tobacco smoke: Emerging evidence and arguments for a multidisciplinary research agenda. *Environ. Health Perspect.* **2011**, *119*, 1218–1226. [[CrossRef](#)]
10. Matt, G.E.; Quintan, P.J.; Zakarian, J.M.; Fortmann, A.L.; Chatfield, D.A.; Hoh, E.; Uribe, A.M.; Hovell, M.F. When smokers move out and non-smokers move in: Residential thirdhand smoke pollution and exposure. *Tob. Control* **2011**, *20*, e1. [[CrossRef](#)]
11. Sleiman, M.; Logue, J.M.; Luo, W.; Pankow, J.F.; Gundel, L.A.; Destailats, H. Inhalable Constituents of Thirdhand Tobacco Smoke: Chemical Characterization and Health Impact Considerations. *J. Environ. Sci. Technol.* **2014**, *48*, 13093–13101. [[CrossRef](#)] [[PubMed](#)]
12. Bahl, V.; Jacob, P., III; Havel, C.; Schick, S.F.; Talbot, P. Thirdhand cigarette smoke: Factors affecting exposure and remediation. *PLoS ONE* **2014**, *9*, e108258. [[CrossRef](#)] [[PubMed](#)]
13. Bahl, V.; Shim, H.J.; Payton, J., III; Dias, K.; Schick, S.F.; Talbot, P. Thirdhand Smoke: Chemical dynamics, cytotoxicity, and genotoxicity in outdoor and indoor environments. *Toxicol. In Vitro* **2016**, *32*, 220–231. [[CrossRef](#)]
14. Pozuelos, G.L.; Jacob, P., III; Schick, S.F.; Omaiye, E.E.; Talbot, P. Adhesion and Removal of Thirdhand Smoke from Indoor Fabrics: A Method for Rapid Assessment and Identification of Chemical Repositories. *Int. J. Environ. Res. Public Health* **2021**, *18*, 3592. [[CrossRef](#)] [[PubMed](#)]
15. Northrup, T.; Khan, A.M.; Jacob, P., III; Benowitz, N.L.; Hoh, E.; Hovell, M.F.; Matt, G.E.; Stotts, A.L. Thirdhand smoke contamination in hospital settings: Assessing exposure risk for vulnerable pediatric patients. *Tob. Control* **2016**, *25*, 619–623. [[CrossRef](#)]

16. Matt, G.E.; Quintana, P.J.; Hovell, M.F.; Bernert, J.T.; Song, S.; Novianti, N.; Juarez, T.; Floro, J.; Gehrman, C.; Garcia, M.; et al. Households contaminated by environmental tobacco smoke: Sources of infant exposures. *Tob. Control* **2004**, *13*, 29. [[CrossRef](#)] [[PubMed](#)]
17. Omaiye, E.E.; McWhirter, K.J.; Luo, W.; Pankow, J.F.; Talbot, P. High-Nicotine Electronic Cigarette Products: Toxicity of JUUL Fluids and Aerosols Correlates Strongly with Nicotine and Some Flavor Chemical Concentrations. *Chem. Res. Toxicol.* **2019**, *32*, 1058–1069. [[CrossRef](#)]
18. Omaiye, E.E.; McWhirter, K.J.; Luo, W.; Tierney, P.A.; Pankow, J.F.; Talbot, P. High concentrations of flavor chemicals are present in electronic cigarette refill fluids. *Sci. Rep.* **2019**, *9*, 2468. [[CrossRef](#)]
19. Davis, B.; Dang, M.; Kim, J.; Talbot, P. Nicotine concentrations in electronic cigarette refill and do-it-yourself fluids. *Nicotine Tob. Res.* **2015**, *17*, 134–141. [[CrossRef](#)]
20. Trtchounian, A.; Talbot, P. Electronic nicotine delivery systems: Is there a need for regulation? *Tob. Control* **2010**, *20*, 47–52. [[CrossRef](#)]
21. Garcia, R.; Allem, J.P.; Baezconde-Garbanati, L.; Unger, J.B.; Sussman, S. Employee and customer handling of nicotine-containing e-liquids in vape shops. *Tob. Prev. Cessat* **2016**, *2*, 1–10. [[CrossRef](#)] [[PubMed](#)]
22. Cantrell, F.L. Adverse effects of e-cigarette exposures. *J. Community Health* **2014**, *39*, 614–616. [[CrossRef](#)] [[PubMed](#)]
23. Khachatoorian, C.; Jacob, P., III; Sen, A.; Zhu, Y.; Benowitz, N.L.; Talbot, P. Identification and quantification of electronic cigarette exhaled aerosol residue chemicals in field sites. *Environ. Res.* **2019**, *170*, 351–358. [[CrossRef](#)] [[PubMed](#)]
24. Maina, G.; Castagnoli, C.; Ghione, G.; Passini, V.; Adami, G.; Filon, F.L.; Crosera, M. Skin contamination as pathway for nicotine intoxication in vapers. *Toxicol. In Vitro.* **2017**, *17*, 30061–30069. [[CrossRef](#)]
25. Casas, J.W.; Lewerenz, G.M.; Rankin, E.A.; Willoughby, J.A.; Blakeman, L.C.; McKim, J.M.; Coleman, K.P. In vitro human skin irritation test for evaluation of medical device extracts. *Toxicol. In Vitro.* **2013**, *27*, 2175–2183. [[CrossRef](#)]
26. Kandárová, H.; Willoughby, J.A.; De Jong, W.H.; Letasiova, S.; Milasova, T.; Bachelor, M.A.; Breyfogle, B.; Handa, Y.; De La Fonteyne, L.; Coleman, K.P. Pre-validation of an in vitro skin irritation test for medical devices using the reconstructed human tissue model EpiDermTM. *Toxicol. In Vitro.* **2018**, *50*, 407–417. [[CrossRef](#)]
27. Hughes, C.S.; Foehr, S.; Garfield, D.A.; Furlong, E.E.; Steinmetz, L.M.; Krijgsveld, J. Ultrasensitive proteome analysis using paramagnetic bead technology. *Mol. Syst. Biol.* **2014**, *10*, 757. [[CrossRef](#)]
28. Deng, W.; Sha, J.; Plath, K.; Wohlschlegel, J.A. Carboxylate-Modified Magnetic Bead (CMMB)-Based Isopropanol Gradient Peptide Fractionation (CIF) Enables Rapid and Robust Off-Line Peptide Mixture Fractionation in Bottom-Up Proteomics. *Mol. Cell. Proteom.* **2021**, *20*, 100039. [[CrossRef](#)]
29. Cox, J.; Mann, M. MaxQuant enables high peptide identification rates, individualized p.p.b.-range mass accuracies and proteome-wide protein quantification. *Nat. Biotechnol.* **2008**, *26*, 1367–1372. [[CrossRef](#)]
30. Huang, T.; Choi, M.; Tzouros, M.; Golling, S.; Pandya, N.J.; Banfai, B.; Dunkley, T.; Vitek, O. MSstatsTMT: Statistical Detection of Differentially Abundant Proteins in Experiments with Isobaric Labeling and Multiple Mixtures. *Mol. Cell. Proteom.* **2020**, *19*, 1706–1723. [[CrossRef](#)]
31. Abramoff, M.D.; Magalhaes, P.J.; Ram, S.J. Image Processing with Image. *J. Biophotonics Int.* **2004**, *11*, 36–42.
32. Chen, H.; Detmer, S.A.; Ewald, A.J.; Griffin, E.E.; Fraser, S.E.; Chan, D.C. Mitofusins Mfn1 and Mfn2 coordinately regulate mitochondrial fusion and are essential for embryonic development. *J. Cell Biol.* **2003**, *160*, 189–200. [[CrossRef](#)] [[PubMed](#)]
33. Ganguli, G.; Mukherjee, U.; Sonawane, A. Peroxisomes and Oxidative Stress: Their Implications in the Modulation of Cellular Immunity During Mycobacterial Infection. *Front. Microbiol.* **2019**, *10*, 1121. [[CrossRef](#)] [[PubMed](#)]
34. Tsoyi, K.; Jang, H.J.; Kim, J.W.; Chang, H.K.; Lee, Y.S.; Pae, H.O.; Kim, H.J.; Seo, H.G.; Lee, J.H.; Chung, H.T.; et al. Stimulation of alpha7 nicotinic acetylcholine receptor by nicotine attenuates inflammatory response in macrophages and improves survival in experimental model of sepsis through heme oxygenase-1 induction. *Antioxid. Redox Signal* **2011**, *14*, 2057–2070. [[CrossRef](#)]
35. Kalra, R.; Singh, S.P.; Pena-Philippides, J.C.; Langley, R.J.; Razani-Boroujerdi, S.; Sopori, M.L. Immunosuppressive and anti-inflammatory effects of nicotine administered by patch in an animal model. *Clin. Diagn. Lab Immunol.* **2004**, *11*, 563–568. [[CrossRef](#)]
36. Staples, J.; Klein, D. Can nicotine use alleviate symptoms of psoriasis? *Can. Fam. Physician* **2012**, *58*, 404–408.
37. Scott, D.A.; Martin, M. Exploitation of the nicotinic anti-inflammatory pathway for the treatment of epithelial inflammatory diseases. *World J. Gastroenterol.* **2006**, *12*, 7451–7459. [[CrossRef](#)]
38. Misery, L. Nicotine effects on skin: Are they positive or negative? *Exp. Dermatol.* **2004**, *13*, 665–670. [[CrossRef](#)]
39. Ingram, J.R. Nicotine: Does it have a role in the treatment of skin disease? *Postgrad. Med. J.* **2009**, *85*, 196–201. [[CrossRef](#)]
40. Stegemann, A.; Böhm, M. Targeting the $\alpha 7$ nicotinic acetylcholine receptor—A novel road towards the future treatment of skin diseases. *Exp. Dermatol.* **2020**, *29*, 924–931. [[CrossRef](#)]
41. Radek, K.A.; Elias, P.M.; Taupenot, L.; Mahata, S.K.; O'Connor, D.T.; Gallo, R.L. Neuroendocrine nicotinic receptor activation increases susceptibility to bacterial infections by suppressing antimicrobial peptide production. *Cell Host Microbe* **2010**, *7*, 277–289. [[CrossRef](#)] [[PubMed](#)]
42. Kishibe, M.; Griffin, T.M.; Radek, K.A. Keratinocyte nicotinic acetylcholine receptor activation modulates early TLR2-mediated wound healing responses. *Int. Immunopharmacol.* **2015**, *29*, 63–70. [[CrossRef](#)] [[PubMed](#)]
43. Cañe-Dorantes, L.; Cañedo-Ayala, M. Skin acute wound healing: A comprehensive review. *Int. J. Inflamm.* **2019**, *2019*, 3706315. [[CrossRef](#)]

44. Koh, T.J.; DiPietro, L.A. Inflammation and wound healing: The role of the macrophage. *Expert Rev. Mol. Med.* **2011**, *13*, e23. [[CrossRef](#)] [[PubMed](#)]
45. Seeger, M.A.; Paller, A.S. The Roles of Growth Factors in Keratinocyte Migration. *Adv. Wound Care* **2015**, *4*, 213–224. [[CrossRef](#)] [[PubMed](#)]
46. Chernyavsky, A.I.; Arredondo, J.; Qian, J.; Galitovskiy, V.; Grando, S.A. Coupling of ionic events to protein kinase signaling cascades upon activation of alpha7 nicotinic receptor: Cooperative regulation of alpha2-integrin expression and Rho kinase activity. *J. Biol. Chem.* **2009**, *284*, 22140–22148. [[CrossRef](#)]
47. Chernyavsky, A.I.; Arredondo, J.; Marubio, L.M.; Grando, S.A. Differential regulation of keratinocyte chemokinesis and chemotaxis through distinct nicotinic receptor subtypes. *J. Cell Sci.* **2004**, *117*, 5665–5679. [[CrossRef](#)]
48. Martins-Green, M.; Adhami, N.; Frankos, M.; Valdez, M.; Goodwin, B.; Lyubovitsky, J.; Dhall, S.; Garcia, M.; Egiebor, I.; Martinez, B.; et al. Cigarette smoke toxins deposited on surfaces: Implications for human health. *PLoS ONE* **2014**, *9*, e86391. [[CrossRef](#)]
49. Liu, B.; Qian, S.B. Translational reprogramming in cellular stress response. *Wiley Interdiscip. Rev. RNA* **2014**, *5*, 301–315. [[CrossRef](#)]
50. Warnakulasuriyarachchi, D.; Cerquozzi, S.; Cheung, H.H.; Holcik, M. Translational induction of the inhibitor of apoptosis protein HIAP2 during endoplasmic reticulum stress attenuates cell death and is mediated via an inducible internal ribosome entry site element. *J. Biol. Chem.* **2004**, *279*, 17148–17157. [[CrossRef](#)]
51. Huang, W.; Placzek, A.N.; Viana Di Prisco, G.; Khatiwada, S.; Sidrauski, C.; Krnjević, K.; Walter, P.; Dani, J.A.; Costa-Mattioli, M. Translational control by eIF2 α phosphorylation regulates vulnerability to the synaptic and behavioral effects of cocaine. *Elife* **2016**, *5*, e12052. [[CrossRef](#)] [[PubMed](#)]
52. Wong, M.K.; Holloway, A.C.; Hardy, D.B. Nicotine directly induces endoplasmic reticulum stress response in rat placental trophoblast giant cells. *Toxicol. Sci.* **2016**, *151*, 23–34. [[CrossRef](#)] [[PubMed](#)]
53. Placzek, A.N.; Molfese, D.L.; Khatiwada, S.; Di Prisco, G.V.; Huang, W.; Sidrauski, C.; Krnjević, K.; Amos, C.L.; Ray, R.; Dani, J.A.; et al. Translational control of nicotine-evoked synaptic potentiation in mice and neuronal responses in human smokers by eIF2 α . *Elife* **2016**, *5*, e12056. [[CrossRef](#)] [[PubMed](#)]
54. Hong, M.; Kim, H.; Kim, I. Ribosomal protein L19 overexpression activates the unfolded protein response and sensitizes MCF7 breast cancer cells to endoplasmic reticulum stress-induced cell death. *Biochem. Biophys. Res. Commun.* **2014**, *450*, 673–678. [[CrossRef](#)]
55. Meng, T.T.; Wang, W.; Meng, F.L.; Wang, S.Y.; Wu, H.H.; Chen, J.M.; Zheng, Y.; Wang, G.X.; Zhang, M.X.; Li, Y.; et al. Nicotine Causes Mitochondrial Dynamics Imbalance and Apoptosis Through ROS Mediated Mitophagy Impairment in Cardiomyocytes. *Front Physiol.* **2021**, *12*, 650055. [[CrossRef](#)]
56. Zahedi, A.; Phandthong, R.; Chaili, A.; Leung, S.; Omaiye, E.; Talbot, P. Mitochondrial Stress Response in Neural Stem Cells Exposed to Electronic Cigarettes. *iScience* **2019**, *16*, 250–269. [[CrossRef](#)]
57. Grando, S.A.; Horton, R.M.; Mauro, T.M.; Kist, D.A.; Lee, T.X.; Dahl, M.V. Activation of keratinocyte nicotinic cholinergic receptors stimulates calcium influx and enhances cell differentiation. *J. Investig. Dermatol.* **1996**, *107*, 412–418. [[CrossRef](#)]
58. Hirata, N.; Yamada, S.; Asanagi, M.; Sekino, Y.; Kanda, Y. Nicotine induces mitochondrial fission through mitofusin degradation in human multipotent embryonic carcinoma cells. *Biochem. Biophys. Res. Commun.* **2016**, *470*, 300–305. [[CrossRef](#)]
59. Bahl, V.; Johnson, K.; Phandthong, R.; Zahedi, A.; Schick, S.F.; Talbot, P. Thirdhand cigarette smoke causes stress-induced mitochondrial hyperfusion and alters the transcriptional profile of stem cells. *Toxicol. Sci.* **2016**, *153*, 55–69. [[CrossRef](#)]
60. Pascual-Ahuir, A.; Manzanares-Estreder, S.; Proft, M. Pro- and Antioxidant Functions of the Peroxisome-Mitochondria Connection and Its Impact on Aging and Disease. *Oxid. Med. Cell. Longev.* **2017**, *2017*, 9860841. [[CrossRef](#)]
61. Tripathi, D.N.; Walker, C.L. The peroxisome as a cell signaling organelle. *Curr. Opin. Cell Biol.* **2016**, *39*, 109–112. [[CrossRef](#)] [[PubMed](#)]
62. Till, A.; Lakhani, R.; Burnett, S.F.; Subramani, S. Pexophagy: The selective degradation of peroxisomes. *Int. J. Cell Biol.* **2012**, *2012*, 512721. [[CrossRef](#)] [[PubMed](#)]
63. Zhang, J.; Tripathi, D.N.; Jing, J.; Alexander, A.; Kim, J.; Powell, R.T.; Dere, R.; Tait-Mulder, J.; Lee, J.H.; Paull, T.T.; et al. ATM functions at the peroxisome to induce pexophagy in response to ROS. *Nat. Cell Biol.* **2015**, *17*, 1259–1269. [[CrossRef](#)] [[PubMed](#)]
64. Jean Beltran, P.M.; Cook, K.C.; Hashimoto, Y.; Galitzine, C.; Murray, L.A.; Vitek, O.; Cristea, I.M. Infection-Induced Peroxisome Biogenesis Is a Metabolic Strategy for Herpesvirus Replication. *Cell. Host Microbe* **2018**, *24*, 526–541.e7. [[CrossRef](#)]
65. Baumgart, E.; Vanhorebeek, I.; Grabenbauer, M.; Borgers, M.; Declercq, P.E.; Fahimi, H.D.; Baes, M. Mitochondrial alterations caused by defective peroxisomal biogenesis in a mouse model for Zellweger syndrome (PEX5 knockout mouse). *Am. J. Pathol.* **2001**, *159*, 1477–1494. [[CrossRef](#)]
66. Huang, K.; Kim, J.; Vo, P.; Miao, T.; Bai, H. Peroxisome import stress impairs ribosome biogenesis and induces integrative stress response through eIF2 α phosphorylation. *bioRxiv* **2020**. [[CrossRef](#)]
67. Kim, J.; Bai, H. Peroxisomal Stress Response and Inter-Organelle Communication in Cellular Homeostasis and Aging. *Antioxidants* **2022**, *11*, 192. [[CrossRef](#)]
68. Kovacs, W.J.; Charles, K.N.; Walter, K.M.; Shackelford, J.E.; Wikander, T.M.; Richards, M.J.; Fliesler, S.J.; Krisans, S.K.; Faust, P.L. Peroxisome deficiency-induced ER stress and SREBP-2 pathway activation in the liver of newborn PEX2 knock-out mice. *Biochim. Biophys. Acta* **2012**, *1821*, 895–907. [[CrossRef](#)]

69. Piao, L.; Dorotea, D.; Jiang, S.; Koh, E.H.; Oh, G.T.; Ha, H. Impaired Peroxisomal Fitness in Obese Mice, a Vicious Cycle Exacerbating Adipocyte Dysfunction via Oxidative Stress. *Antioxid. Redox Signal* **2019**, *31*, 1339–1351. [[CrossRef](#)]
70. Ahlemeyer, B.; Gottwald, M.; Baumgart-Vogt, E. Deletion of a single allele of the Pex11 β gene is sufficient to cause oxidative stress, delayed differentiation and neuronal death in mouse brain. *Dis. Model Mech.* **2012**, *5*, 125–140. [[CrossRef](#)]
71. López-Erauskin, J.; Galino, J.; Ruiz, M.; Cuezva, J.M.; Fabregat, I.; Cacabelos, D.; Boada, J.; Martínez, J.; Ferrer, I.; Pamplona, R.; et al. Impaired mitochondrial oxidative phosphorylation in the peroxisomal disease X-linked adrenoleukodystrophy. *Hum. Mol. Genet.* **2013**, *22*, 3296–3305. [[CrossRef](#)] [[PubMed](#)]
72. Pozuelos, G.L.; Kagda, M.S.; Schick, S.; Girke, T.; Volz, D.C.; Talbot, P. Experimental Acute Exposure to Thirdhand Smoke and Changes in the Human Nasal Epithelial Transcriptome: A Randomized Clinical Trial. *JAMA Netw. Open* **2019**, *2*, e196362. [[CrossRef](#)] [[PubMed](#)]